DOI: 10.13009/EUCASS2017-184

Multi-objective morphing wing optimization for an Unmanned Air Vehicle

Durmuş Sinan Körpe and Serkan Özgen***
**Aeronautical Engineering Department, University of Turkish Aeronautical Association*
Bahçekapı Mahallesi, Okul Sokak No:11, Etimesgut, Ankara, Turkey
***Aerospace Engineering Department, Middle East Technical University*
Üniversiteler Mahallesi, Dumlupınar Bulvarı No:1, 06800 Çankaya, Ankara, Turkey

Abstract
This work describes the optimization process of a morphing wing for an unmanned air vehicle (UAV) by using multi-objective gradient based optimization algorithm in which maximization of lift to drag ratio and minimization of bending moment at wing root chord plane are defined as the objective functions. Six different optimization problems are solved by changing weighted sum coefficients of the objective functions in order to observe the morphing wing planform and the airfoil shape change. According to the results, 15.2% lift to drag ratio increase is obtained while the increase in the bending moment is 2%.

1. Introduction

In most of the aerodynamic shape optimization studies of the morphing wing concepts, it is pointed out that the span increases when the aircraft is flying with a speed that is close to the stall speed of the original wing [1, 2]. When a morphing wing increases the span, the wing area and the aspect ratio increases and this yields less induced drag. Contrary to this, wing-root bending moment will increase with increasing span and a heavier wing structure will be a consequence. Since most of the morphing wing applications are based on variable span, it is important to investigate the pros and cons of it. The dilemma that is mentioned above is not an issue only for morphing wing design. In the design process of the fixed wing aircraft, the designers consider the wing-root bending moment change either by defining it as an objective function or as a functional constraint as Lyu and Martins do [3]. In the first problem in their studies, drag is defined as the objective function and lift is designed as functional equality constraint. 251 design variables are used in the optimization problem and 30.7% drag reduction is obtained when the aircraft speed is $M = 0.85$. However, when center plane bending moment and trim are defined as equality constraints to the first problem, drag reduction is 27.4% [3]. In the study of Bae et al. that is related with variable span morphing wing, the tip deflection and divergence speed of the morphing wing at different span extension ratios are measured. According to the results, it is stated that the morphing wing designers should take larger bending stiffness into account in structural design because the wing deformation due to bending is much more significant than twist [4].

In this study, the UAV that is going to have the morphing wing mechanism, OPT, is optimized at first. This optimization problem includes aircraft lift to drag ratio, L/D, maximization as the objective function. Minimum speed, V_1, and maximum speed, V_3, of the base UAV, BASE, are defined as inequality constraints so that OPT can satisfy level flight at these speeds. After that, the multi-objective morphing wing optimization problem is defined. In this problem, both maximization of L/D and minimization of bending moment around the root chord plane are defined as objective functions by using the weighted sum method. Six different optimization problems are solved by changing the weighting coefficients. The aerodynamic design tool consists of the three-dimensional panel method, two-dimensional boundary layer solution and generalized reduced gradient method-based optimization algorithm. Wing lift, L_w, wing-induced drag, D_{wi}, and wing pressure drag, D_{wp}, are obtained by using the three-dimensional panel method, which is a first-order method and consists of constant strength sources and doublets. Wing skin friction drag, D_{wf}, is calculated by using the two-dimensional laminar and turbulent boundary layer models of Thwaites and Head, respectively. Aerodynamic forces on horizontal tail, vertical tail and body are calculated by conceptual design empirical formulas. Generalized reduced gradient method algorithm is used as the optimization solver.

Copyright © 2017 by First Author and Second Author. Published by the EUCASS association with permission.

DOI: 10.13009/EUCASS2017-184

2. Method

2.1 Aerodynamic calculations of the wing

L_w, D_{wi}, and D_{wp} are obtained by using the three-dimensional panel method whose results are consistent with XFLR5 results [5]. D_{wf} is calculated by using the two-dimensional laminar and turbulent boundary layer models of Thwaites and Head, respectively. In order to include the effect of the turbulent separation on drag increase, skin friction coefficient, C_f, values that are downstream of the separation location are taken as 1.02 times higher than the previous panel skin friction coefficient value, if separation develops before 98% of the chord. Equation 1 and Equation 2 are used in order to include the turbulent separation to drag increase and lift decrease for the lift, L_{wst}, and drag, D_{wst}, value of each wing strip [1].

$$D_{wst} = D_{wst} \cdot \left(\frac{\frac{x_{te}}{c}}{\frac{x_{sep}}{c}} \right) \tag{1}$$

$$L_{wst} = L_{wst} \cdot \left[1 - 0.5 \cdot \left(\frac{x_{te}}{c} - \frac{x_{sep}}{c} \right) \right] \tag{2}$$

In above equations x_{te}/c is the non-dimensional trailing edge length whereas x_{sep}/c non-dimensional distance of turbulent separation point with respect to the leading edge of the strip. When the results of the developed boundary layer solver are compared with XFOIL's results for NACA 4412, higher C_f calculation of the developed boundary solver is observed at all angle of attacks. But it is noticed that this situation enforces the optimization solver to create smoother airfoil surfaces. Therefore, the corrections equations are continued to be used as they are [1].

2.2 Aerodynamic calculations of other UAV components

Total drag of the UAV, D, consists of wing drag, zero lift drag, D_{0c}, and drag due to lift, D_{Lc}, of the UAV components except the wing. Zero lift drag coefficient of the UAV without wing, C_{D0c}, is found according to Equation 3 [6].

$$C_{D0c} = \frac{C_{fht} \cdot FF_{ht} \cdot Q_{ht} \cdot S_{wetht} + C_{fvt} \cdot FF_{vt} \cdot Q_{vt} \cdot S_{wetvt} + C_{fb} \cdot FF_b \cdot Q_b \cdot S_{wetb}}{S_w} \tag{3}$$

In above equation, the subscript ht, vt, and b are for horizontal tail, vertical tail, and body, respectively. It is assumed that flow around the components are turbulent and turbulent flow flat plate skin friction coefficient is used as shown in Equation 4, in the calculations for this study.

$$C_f = \frac{0.455}{(log_{10}Re)^{2.58}(1 + 0.144M^2)^{0.65}} \tag{4}$$

In Equation 4, Re is calculated according to the characteristic length of the component that is the standard mean aerodynamic chord length for the tail surfaces, whereas it is total length for the body. Form factor, FF, for the tail surfaces is calculated by using Equation 5 [6].

$$FF = \left(1 + \frac{0.6}{(x/c)_m} \cdot \left(\frac{t}{c} \right) + 100 \cdot \left(\frac{t}{c} \right)^4 \right) \cdot (1.35 \cdot M^{0.18} \cdot (cos\, \Lambda_m)^{0.28}) \tag{5}$$

Q term is the interference factor and it is 1.03 for the tails. Equation 6 and Equation 7 are used for wetted area calculation for horizontal tail, S_{wetht}, and the vertical tail, S_{wetvt}.

$$S_{wetht} = S_{ht} \cdot \left(1.977 + 0.52 \cdot \left(\frac{t}{c} \right) \right) \tag{6}$$

$$S_{wetwt} = S_{wt} \cdot \left(1.977 + 0.52 \cdot \left(\frac{t}{c} \right) \right) \tag{7}$$

DOI: 10.13009/EUCASS2017-184

The geometric data of the tails that are used in above equations are defined in Table 1. These are the volume coefficient, c, the moment arm distance, which is the length between the aerodynamic center of the wing and the aerodynamic center of the tail, $\bar{L}$, planform area, S, aspect ratio, AR, taper ratio, λ, airfoil of tails and sweep angle of the maximum thickness line, Λ_m. The airfoil of the tails is NACA012 that has a maximum thickness value, t/c, of 12% at 30% of the airfoil, which is the chord wise location of the maximum thickness of the airfoil, $(x/c)_m$.

Table 1: Geometric data of the horizontal and the vertical tail of BASE

	Horizontal tail	Vertical tail
c	0.5	0.04
$\bar{L}$ (m)	1.8	1.8
S (m^2)	$\frac{c_{ht} \cdot S_w \cdot \bar{c}_w}{\bar{L}_{ht}} = \frac{S_w}{3.6} \cdot \left(\frac{2 \cdot c_{rw}}{3} \cdot \frac{1 + \lambda_w + \lambda_w^2}{1 + \lambda_w} \right)$	$\frac{c_{vt} \cdot S_w \cdot b_w}{\bar{L}_{vt}} = \frac{S_w \cdot b_w}{45}$
AR	$\frac{2 \cdot AR_w}{3}$	1.5
λ	0.6	0.5
Λ_m (°)	0°	20°
Airfoil	NACA0012	NACA0012
$(x/c)_m$	30%	30%
t/c	12%	12%

As it is seen in Table 1, S and AR of the horizontal tail and S of the vertical tail are dependent on the wing area, S_w, wing root chord, c_{rw}, wing taper ratio, λ_w, and wing span, b_w. In order to investigate the drag due to lift characteristic of the tail, level flight condition of the UAV is investigated. At level flight, summation of L_w and the horizontal tail lift, L_{ht}, is equal to weight of the UAV, W. In addition to this, longitudinal moment around center of gravity of the UAV is zero. It is assumed that the center of gravity of the UAV, which does not change during optimization process, is 0.1 m ahead of the aerodynamic center of the wing. For this analysis, the effect of body on lift is neglected. After the mathematical definition of the level flight condition, L_w and L_{ht} are found by using Equations 8 and 9.

$$L_w = \frac{19 \cdot W}{18} \tag{8}$$

$$L_{ht} = -\frac{L_w}{19} \tag{9}$$

The former equation is used for the definition of the level flight in optimization problems. Induced drag coefficient of the horizontal tail that is in Equation 10 is calculated by using the latter equation.

$$C_{DLht} = \frac{\left(\frac{2 \cdot L_w}{19 \cdot \rho \cdot S_{ht} \cdot V^2} \right)^2 \cdot S_{ht}}{\pi \cdot e_{ht} \cdot AR_{ht} \cdot S_w} \tag{10}$$

In the above equation, C_{DLht} defines drag due to lift coefficient of the horizontal tail. e_{ht} is horizontal tail Oswald span efficiency factor and it is taken as 0.9. V is the UAV flight speed. FF is calculated for the body by using Equation 11. Value of Q is 1 for this component.

$$FF = \left(1 + \frac{60}{(l/d_{max})^3} + \frac{(l/d_{max})}{400} \right) \tag{11}$$

The effect of the body on the drag due to lift of the UAV is taken into account in the calculation by using Equation 12 [7].

$$C_{DLb} = 2 \cdot \alpha_b^2 \cdot \frac{S_{bb}}{S_w} + \eta \cdot c_{dc} \cdot |\alpha_b^3| \cdot \frac{S_{bplf}}{S_w} \tag{12}$$

DOI: 10.13009/EUCASS2017-184

C_{DLb} is drag due to lift coefficient of the body and α_b is angle of attack of the body that is assumed as equal to wing angle of attack. The geometric and aerodynamic parameters of the body are in Table 2. l is the length and d_{max} is the diameter of the maximum cross-sectional area of the body. S_{bb} is the cross-sectional area of the most aft portion of the body. η is the ratio of the drag of a finite cylinder to the drag of an infinite cylinder that is a function of l/d_{max}. c_{dc} is the experimental steady state cross-flow drag coefficient of a circular cylinder that is a function of Mach number. S_{bplf} is the top view area of the body.

Table 2: Geometric and aerodynamic parameters of the body

S_{wetb} (m^2)	3
l (m)	3.6
d_{max} (m)	0.36
S_{bb} (m^2)	0.008
η	0.686
c_{dc}	1.2
S_{bplf} (m^2)	1

As a sum, the total drag of the UAV is found as it is shown in Equation …

$$D = D_w + \frac{1}{2} \cdot \rho \cdot V^2 \cdot S_w \cdot (C_{D0c} + C_{DLb} + C_{DLht}) \tag{13}$$

2.2 Optimization solver

The optimization solver, GRGM, is developed by using generalized reduced gradient method and it is verified by comparing it with the optimization solvers by solving a benchmark structural optimization problem in the literature [1]. The subroutines that compute gradient array of objective function and Jacobian matrix of the constraints and selection of the optimum step length are parallelized.

3. Results

3.1 Aerodynamic characteristic of BASE

Geometric data of BASE's components is shown in Table 3. These are c_{rw}, wing tip chord, c_{tw}, b_w, S_w, the horizontal tail root chord, c_{rht}, tip chord, c_{tht}, span, b_{ht}, and planform area, S_{ht}, and the vertical tail root chord, c_{rvt}, tip chord, c_{tvt}, span, b_{vt}, and planform area, S_{vt}.

Table 3: Geometric data of BASE's components.

c_{rw} (m)	0.45
c_{tw} (m)	0.25
b_w (m)	3.5
S_w (m^2)	1.225
c_{rht} (m)	0.169
c_{tht} (m)	0.102
b_{ht} (m)	0.903
S_{ht} (m^2)	0.122
c_{rvt} (m)	0.336
c_{tvt} (m)	0.168
b_{vt} (m)	0.378
S_{vt} (m^2)	0.095

Airfoil of BASE has a maximum thickness of 11.81% at $0.31c$ and 3.93% maximum camber value at $0.45c$ position as it is shown in Figure 1. The airfoil shape is obtained with 11 control points by using b-spline method. Six of them are for thickness generation at $0.001c$, $0.05c$, $0.2c$, $0.5c$, $0.8c$ and $0.95c$ and five of them are for camber generation at $0.05c$, $0.2c$, $0.5c$, $0.8c$ and $0.95c$. Both ends of the curves are clamped.

DOI: 10.13009/EUCASS2017-184

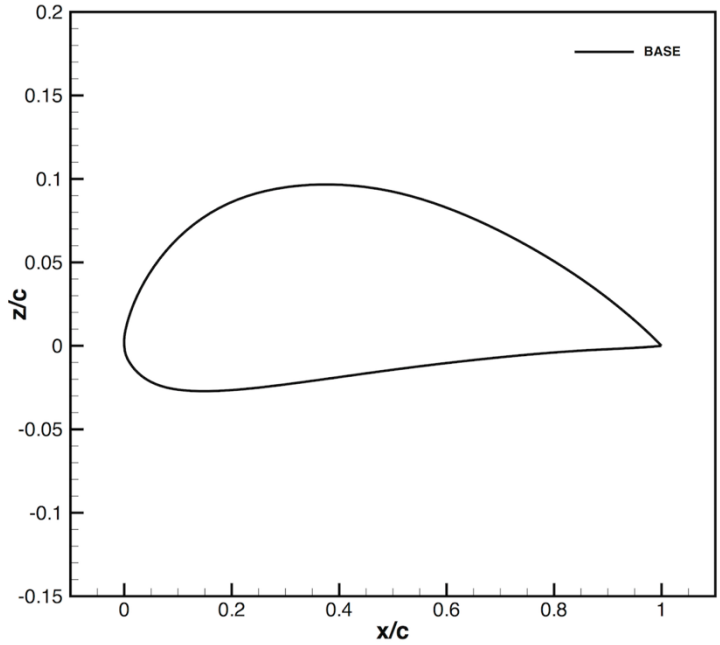

Figure 1: BASE airfoil

The weight of BASE, W, is 300 N and power available, P_A, is 2512.31 N. Table 4 shows the steady level flight characteristic of BASE.

Table 4: Level flight performance of BASE at different speeds

V (m/s)	α (°)	L_{wcal} (N)	$D_{wi} + D_{wp}$ (N)	D_w (N)	D_{0c} (N)	D_{Lc} (N)	D (N)	P_R (W)	L/D
16	14.18	333.94	18.03	20.45	2.22	2.88	25.54	408.71	11.74
19	8.10	320.41	11.81	14.17	3.05	1.13	18.35	348.72	16.35
22	4.80	318.12	8.73	10.97	4.01	0.58	15.56	342.33	19.28
25	2.69	317.75	6.78	9.37	5.09	0.36	14.82	370.45	20.25
28	1.22	317.39	5.41	8.39	6.28	0.26	14.93	417.96	20.10
31	0.17	317.45	4.41	8.15	7.60	0.20	15.95	494.54	18.81
34	-0.61	317.42	3.65	8.33	9.02	0.17	17.53	595.88	17.12
37	-1.22	317.15	3.04	8.57	10.57	0.16	19.29	713.70	15.55
40	-1.69	317.22	2.56	10.64	12.22	0.16	23.02	920.91	13.03
43	-2.07	317.28	2.15	11.93	13.99	0.17	26.09	1121.98	11.50
46	-2.37	317.37	1.81	12.02	15.87	0.20	28.10	1292.55	10.68
49	-2.62	317.46	1.50	12.90	17.86	0.25	31.00	1519.22	9.68
52	-2.83	317.48	1.23	14.24	19.96	0.30	34.50	1793.84	8.70
55	-3.00	317.31	0.99	15.79	22.17	0.37	38.33	2108.07	7.83
58	-3.15	317.31	0.76	18.39	24.48	0.44	43.32	2512.31	6.93

Before going into details of the above table, it should be mentioned that the wing of BASE should create a lift force, that is equal to $19W/18$ which yields 316.66 N so that level flight condition is satisfied. At 16 m/s, the wing lift decreases from 333.94 N to 316.66 N due to lift correction equation that takes turbulent flow separation, which is $0.88c$ at 14.18°, into account. Power required, P_R, at this speed is less than P_A. As a result, V_1 is 16 m/s. It should be noticed that BASE can perform level flight at 16 m/s with an angle of attack value of 14.18°. The upper limit of angle of attack values in the optimization problems is 15°. That means the minimum speed of BASE is less than 16 m/s. However, in this study the minimum integer speed that satisfies the level flight is defined as the minimum speed. Maximum L/D value is obtained when BASE is flying at 25 m/s, V_2. V_3 is 58 m/s.

DOI: 10.13009/EUCASS2017-184

3.2 Optimization of OPT

Mathematical definition of the optimization problem for L/D maximization of OPT is defined between Equation 14 and Equation 24.

$$\text{Minimize f} = \left(-\frac{L/D}{20.25}\right) \text{ at } \mathrm{V}_2 \tag{14}$$

$$\frac{V_1}{16} - 1 \leq 0 \tag{15}$$

$$1 - \frac{V_3}{58} \leq 0 \tag{16}$$

$$\frac{L_w}{316.66} - 1 = 0 \quad at \ V_3 \tag{17}$$

$$-5^o \leq \alpha_1, \alpha_2, \alpha_3 \leq 15^o \tag{18}$$

$$\frac{z_1}{c} - 0.001 \geq 0 \tag{19}$$

$$\frac{z_6}{c} - 0.01 \geq 0 \tag{20}$$

$$\frac{z_i}{c} \geq 0 \ i = 2 - 5, 7 - 11 \tag{21}$$

$$\frac{z_i}{c} - 0.1 \leq 0 \ i = 1 - 11 \tag{22}$$

$$0.15 \ m \leq c_{rw}, c_{tw} \leq 0.6 \ m \tag{23}$$

$$2.4 \ m \leq b_w \leq 5 \ m \tag{24}$$

The maximization of L/D ratio at V_2 is defined as objective function, f, which is in Equation 14. It is scaled with the highest L/D ratio of BASE. Calculation of V_2 is shown in Equation 25.

$$V_2 = \left(\frac{2 \cdot \left(\frac{19 \cdot W}{18}\right)}{\rho \cdot S_w \cdot C_{Lw}}\right)^{\frac{1}{2}} \tag{25}$$

V_2 is obtained by using the level flight condition equation, which is Equation 8. C_{Lw} is the wing lift coefficient at α_2 angle of attack value. V_1 must be less than or equal to 16 m/s according to Equation 15 and calculation of it is shown in Equation 26.

$$V_1 = \left(\frac{2 \cdot \left(\frac{19 \cdot W}{18}\right)}{\rho \cdot S_w \cdot C_{Lw}}\right)^{\frac{1}{2}} \tag{26}$$

This equation is also defined by the level flight condition equation and C_{Lw} for this speed is calculated by using α_1. V_3 must be greater than or equal to 58 m/s according to the Equation 16. Calculation of this speed includes P_A as it is shown in Equation 27.

DOI: 10.13009/EUCASS2017-184

$$V_3 = \left(\frac{2 \cdot P_A}{\rho \cdot S_w \cdot C_D}\right)^{\frac{1}{3}} \tag{27}$$

The level flight condition at V_3 is defined by using Equation 17. V_1, V_2, and V_3 values are defined as 16 m/s, 25 m/s, and 58 m/s, respectively at the beginning of the optimization problems. The solver calculates aerodynamic forces of the UAV at different angle of attack values. As geometric parameters of the UAV changes, lift and drag values change. As a result, new V_1, V_2, and V_3 values are obtained. The speed update procedure that is discussed above is not applied during the computation of objective function gradient array and Jacobian matrix of the constraints. Lower limit of non-dimensional z values of control points is defined as 0, except first and sixth control points for thickness generation. Dimensionless z value of the first control point is greater than 0.001 for manufacturability concerns and sixth control point is greater than 0.01 for a smoother leading edge region [2]. Upper limit for the non-dimensional control points is 0.1. c_{rw} and c_{tw} are allowed to vary between 0.15 m and 0.6 m. Lower limit and upper limit of b_w are 2.4 m and 5 m, respectively. The design variables for airfoil shape and wing planform generation and their upper and lower limits are scaled with the values of the design variables at the beginning of optimization problem. The optimization problem is solved in 2.41 h on a 2.4 GHz Intel Core i7, 8 GB 1600 MHz MacBook Pro. Table 5 depicts the aerodynamic data of OPT.

Table 5: Aerodynamic data of OPT

	BASE	**OPT**
Max L/D	20.25	27.47
V_1 (m/s)	16	14.78
V_2 (m/s)	25	18.05
V_3 (m/s)	58	58.27
α_1 (°)	14.18	13.49
α_2 (°)	2.69	2.22
α_3 (°)	-3.15	-4.11

According to the results, it is seen that maximum L/D ratio is increased 35.7%. The speed at which maximum L/D is obtained decreases from 25 m/s to 18.05 m/s. OPT can perform level flight with a speed of 14.83 m/s that is less than V_1 of BASE. Since OPT cannot create enough lift at 14 m/s due to turbulent separation around 0.27c, 15 m/s is the minimum integer speed that satisfies the level flight. Therefore, V_1 of OPT is 15 m/s. Maximum speed of OPT is a little bit higher than maximum speed of BASE. Table 6 shows the geometric data of OPT.

Table 6: Geometric data of OPT

	BASE	**OPT**
c_{rw} (m)	0.45	0.402
c_{tw} (m)	0.25	0.15
b_w (m)	3.5	5
S_w (m^2)	1.225	1.378
c_{rht} (m)	0.169	0.121
c_{tht} (m)	0.102	0.073
b_{ht} (m)	0.903	1.169
S_{ht} (m^2)	0.122	0.113
c_{rvt} (m)	0.336	0.426
c_{tvt} (m)	0.168	0.213
b_{vt} (m)	0.378	0.479
S_{vt} (m^2)	0.095	0.153

According to the results, c_{tw} and b_w reach their lower limit and upper limits, respectively. Due to increase in AR_w, b_{ht} increases although c_{rht} and c_{tht} decrease. All geometric properties of the vertical tail increase because the wing geometric data that amplifies the size of the vertical tail increases. Figure 2 depicts the airfoil of OPT.

DOI: 10.13009/EUCASS2017-184

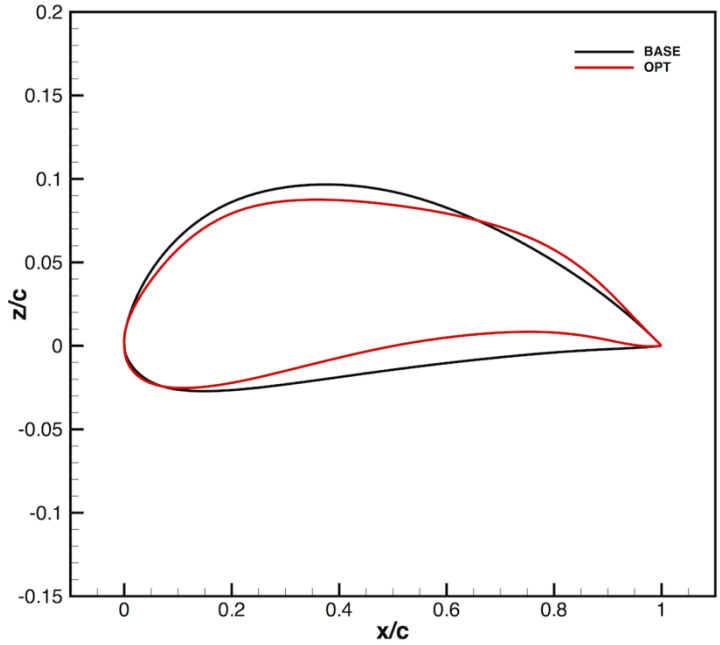

Figure 2: OPT airfoil

Airfoil of OPT has a maximum thickness value of 10.29% at 0.25c. Maximum camber value of it is %4.24 at 0.55c. When it is compared with the airfoil of BASE, maximum thickness decreases and shifts forward, whereas maximum camber increases and shifts reward.

3.2 Multi objective Optimization of Morphing wing

OPT satisfies level flight condition at 15 m/s when angle of attack is 11.57°. L/D value at this speed is 18.47 and bending moment at the root chord plane, M, that is obtained with the multiplication of lift at each panel and normal distance of the panel mid-point to this plane is 175.2 Nm. In this optimization problem, the morphing concept is defined as 20% shape change allowance to both wing planform design variables and airfoil shape design variables. The vertical tail size and the horizontal tail size is not altered in this part. The optimization problem is defined in Equations 28-34.

$$\text{Minimize } \beta_1\left(-\frac{L/D}{18.47}\right)+\beta_2\left(\frac{M}{175.2}\right) \text{ at } 15 \text{ m/s} \tag{28}$$

$$\frac{L_w}{316.66}-1=0 \quad at \ 15 \text{ m/s} \tag{29}$$

$$-5^o \le \alpha_1 \le 15^o \tag{30}$$

$$0.80\left(\frac{Z}{c}\right)_{i,OPT} \le \left|\left(\frac{Z}{c}\right)_i\right| \le 1.2\left(\frac{Z}{c}\right)_{i,OPT} \quad i=1,11 \tag{31}$$

$$0.321\ m \le c_{rw} \le 0.482\ m \tag{32}$$

$$0.12\ m \le c_{rw}, c_{tw} \le 0.18\ m \tag{33}$$

$$4\ m \le b_w \le 6\ m \tag{34}$$

DOI: 10.13009/EUCASS2017-184

The objective function is defined by using weighting coefficients that are β_1 and β_2. Summation of these coefficients are 1. Solution time varies between 0.22 h and 1.1 h. The results of the optimization problem is shown in Table 7.

Table 7: Results of the multi-objective optimization problem.

β_1 - β_2	L/D	M	f_{start}	f_{end}	Change in f
1.0-0.0	24.02	203.74	-1.0	-1.301	30.1%
0.8-0.2	23.88	201.86	-0.6	-0.804	34%
0.6-0.4	23.78	199.72	-0.2	-0.317	58.5%
0.4-0.6	21.28	178.789	0.2	0.151	24.5%
0.2-0.8	13.51	136.65	0.6	0.477	20.5%
0.0-1.0	13.25	135.65	1	0.774	22.6%

The Pareto front of the multi-objective optimization problem in Figure 3 describes the results graphically.

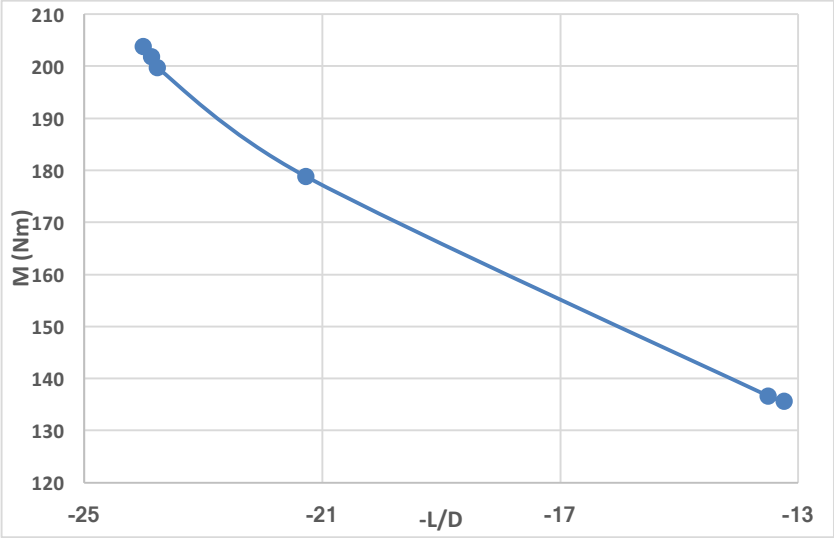

Figure 3: The Pareto front of the multi-objective optimization problem

According to the results, when β_1 is 0.4 and β_2 is 0.6, M value of morphing wing is 2% bigger than the M value of OPT and L/D ratio of morphing wing is 15.2% higher than L/D value of OPT at 15 m/s. As, β_1 gets closer to 1, both L/D and M increase. Although increment in the former value is desirable, increase in the latter value leads to boost in structural weight of the UAV. Table 8 shows the optimum wing planform design variables values.

Table 8: Geometric data of morphing wings.

			β_1 - β_2					
	BASE	**OPT**	**1.0-0.0**	**0.8-0.2**	**0.6-0.4**	**0.4-0.6**	**0.2-0.8**	**0.0-1.0**
c_{rw} (m)	0.45	0.402	0.482	0.48	0.48	0.477	0.482	0.482
c_{tw} (m)	0.25	0.15	0.152	0.138	0.129	0.146	0.126	0.12
b_w (m)	3.5	5	6	6	5.98	5.3	4.01	4
S_w (m^2)	1.225	1.378	1.9	1.854	1.821	1.651	1.219	1.204

According to the results in the table, as β_2 increases wing planform area decreases due to change in b_w. c_{rw} is close to its upper limit. Small alterations form the upper limit are observed for this variable since back to feasible algorithm in GRGM changes the design variables in order to maintain feasibility. c_{tw} decreases as β_1 decreases in the region where $\beta_1$is dominant. This situation is also valid for the region where β_2 is dominant. Figure 4 depicts the optimum airfoils for the multi-objective optimization problem.

DOI: 10.13009/EUCASS2017-184

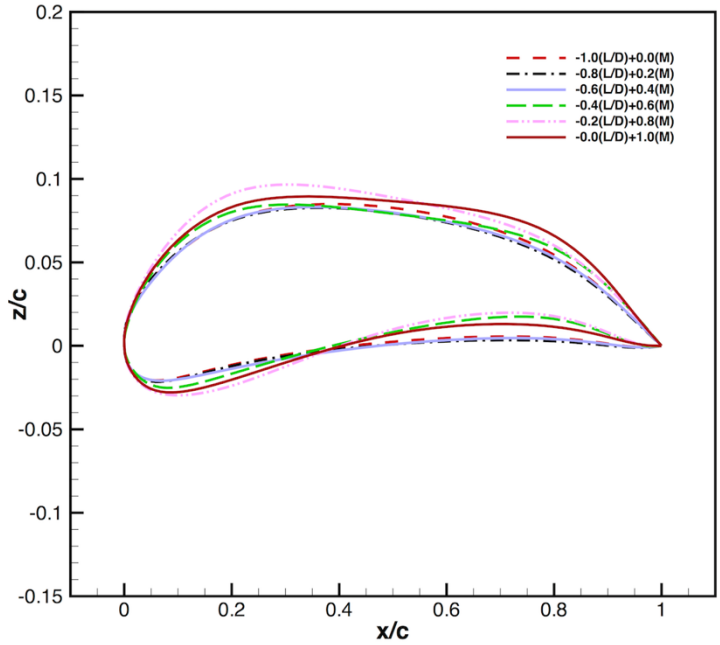

Figure 4: The optimum airfoils of the morphing wings

The optimum airfoils for the region where β_1 is dominant are similar. Camber around the trailing edge region increases in order to create the required lift as β_2 increases, since wing planform area is inversely proportional with β_2.

4. Conclusion

In this study, both fixed wing optimization and morphing wing optimization are performed. In the fixed wing optimization, maximum L/D of the UAV is increased by 35.7%. In addition to this, the optimum UAV can satisfy the level flight performance at the minimum speed and the maximum speed of the base UAV. In the multi-objective morphing wing optimization problem, both maximization of L/D and minimization of bending moment around the root chord plane are defined as objective functions. When β_1 is 0.4 and β_2 is 0.6, the morphing wing has 15.2% higher L/D ratio while the bending moment around the root chord plane is very close to the one that the optimum wing has at 15 m/s.

References

[1] Körpe, D. S., and Özgen, S. 2016. Morphing wing optimization for steady level flight. *Proceedings of the Institution of Mechanical Engineers, Part G: Journal of Aerospace Engineering* First published date: August-21-2016; doi:10.1177/0954410016662063

[2] Gamboa, P., Vale, J., Lau, F. J. P., and Suleman, A. 2009. Optimization of a morphing wing based on coupled aerodynamic and structural constraints. *AIAA Journal*. 47:2087-2104.

[3] Lyu, Z, and Martins, J. 2013. Rans-based aerodynamic shape optimization of a blended-wing-body aircraft. In: *21st AIAA Computational Fluid Dynamics Conference*. AIAA-2013-2586.

[4] Bae, J. S., and Seigler, T. M., and Inman D. J. 2005. Aerodynamic and static aeroelastic characteristics of a variable-span morphing wing. *Journal of Aircraft.* 42:528-534.

[5] Deperrois, A. 2009. About XFLR5 calculations and experimental measurements. *XFLR5 documentation*.

[6] Raymer, D. P. 1992. Aircraft design: a conceptual approach. *2nd ed. Washington: American Institute of Aeronautics and Astronautics Inc*. 280-287.

[7] Roskam, J. 1987. Airplane design, volume vi: preliminary calculation of aerodynamic, thrust, and power characteristics. *1st ed. Kansas: Roskam Aviation and Engineering Corp*. 45-47.